Aerosol characteristics in Phimai, Thailand determined by continuous observation with a polarization sensitive Mie–Raman lidar and a sky radiometer

2015 Environ. Res. Lett. 10 065003

(http://iopscience.iop.org/1748-9326/10/6/065003)

Environmental Research Letters

LETTER

Aerosol characteristics in Phimai, Thailand determined by continuous observation with a polarization sensitive Mie–Raman lidar and a sky radiometer

Nobuo Sugimoto[1], **Atsushi Shimizu**[1], **Tomoaki Nishizawa**[1], **Ichiro Matsui**[1], **Yoshitaka Jin**[1], **Pradeep Khatri**[2], **Hitoshi Irie**[2], **Tamio Takamura**[2], **Kazuma Aoki**[3] **and Boossarasiri Thana**[4]

[1] National Institute for Environmental Studies, 16-2 Onogawa, Tsukuba 305-8506, Japan
[2] Center for Environmental Remote Sensing, Chiba University, 1-33 Yayoi-cho, Inage-ku, Chiba 268-8522, Japan
[3] University of Toyama, 3190 Gofuku, Toyama 930-8555, Japan
[4] Department of Geology, Faculty of Science, Chulalongkorn University, Phayathai Rd, Phathumwan district, Bangkok 10330, Thailand

E-mail: nsugimot@nies.go.jp

Keywords: aerosol, soil dust, biomass burning, aerosol optical characteristics, lidar ratio, Thailand

OPEN ACCESS

RECEIVED
18 January 2015

REVISED
19 April 2015

ACCEPTED FOR PUBLICATION
20 April 2015

PUBLISHED
2 June 2015

Abstract

Distributions and optical characteristics of aerosols were continuously observed with a polarization-sensitive (532 nm), Mie-scattering (532 and 1064 nm) and Raman-scattering (607 nm) lidar and a sky radiometer in Phimai, Thailand. Polarization lidar measurements indicated that high concentration plumes of spherical aerosols considered as biomass burning smoke were often observed in the dry season. Plumes of non-spherical aerosols considered as long-range transported soil dust from Africa, the Middle East, or Northeast Asia were occasionally observed. Furthermore, low-concentration non-spherical aerosols were almost always observed in the atmospheric mixing layer. Extinction coefficient profiles of spherical aerosols and non-spherical dust exhibited different diurnal variations, and spherical aerosols including smoke were distributed in higher altitudes in the mixing layer and residual layer. The difference can be explained by hygroscopic growth of smoke particles and buoyancy of the smoke. Analysis of seasonal variations of optical properties derived from the Raman lidar and the sky radiometer confirmed that the lidar ratio, aerosol optical depth, and Angstrom exponent were higher in the dry season (October–May) and lower in the wet season (June–September). The single scattering albedo was lower in the dry season. These seasonal variations are explained by frequent biomass burning in the dry season consistent with previous studies in Southeast Asian region. At the same time, the present work confirmed that soil dust was a major aerosol component in Phimai, Thailand.

1. Introduction

To clarify the effect of aerosols on climate in Southeast Asia, we conducted long-term observations of aerosols in Thailand. Observations using radiometers and a lidar were initiated in Sri Samrong (99.95 E, 17.15 N) in 1997. The station was moved to Phimai (102.57 E, 15.18 N, 212 m above sea level (ASL)) in 2005. We started our lidar observation with a polarization-sensitive (532 nm) two-wavelength (532, 1064 nm) Mie-scattering lidar, and we added a nitrogen vibrational Raman receiver (607 nm) to the lidar in 2012 to derive the extinction coefficient at 532 nm independently from backscattering. The Phimai station is a SKYNET sky radiometer site (http://atmos.cr.chiba-u.ac.jp) and is a lidar site of the Asian dust and aerosol lidar observation Network (AD-Net) (http://www-lidar.nies.go.jp/AD-Net/) (Sugimoto *et al* 2014). AD-Net is a contributing network to the World Meteorological Organization Global Atmosphere Watch program, and continuous lidar observations are currently performed at 20 locations in East Asia. The data from the AD-Net lidars are processed in near realtime and published on the AD-Net website. The Phimai station is also assigned as an observation site in the United Nations Environment Programme Atmospheric Brown Cloud Project, and observations using various instruments are being conducted (Nakajima *et al* 2007).

Phimai, which is classified as Savanna in Köppen climate classification has a dry season in winter (October–May) and a wet season in summer (June–September). Phimai is located 260 km Northeast of Bangkok in a rural area, with no direct influence of urban and industrial air pollution. Previous studies confirmed that biomass burning is a major source of aerosol in the dry season (Tsuruta *et al* 2009, Campbell *et al* 2012, Li *et al* 2013), though Phimai is located South of significant biomass-burning areas (Campbell *et al* 2012, Lin *et al* 2013). We previously reported that the lidar-observed aerosol optical depth (AOD) in Phimai has a clear correlation with the number of fire hot spots on the Indochina peninsula in the dry season (Shimizu *et al* 2006). Li *et al* (2013) reported on intensive surface observation in the BASE-ASIA campaign in Phimai in the dry season of 2006, and analyzed the chemical composition and size distribution of aerosols. They observed substantial amounts of potassium ions, which suggested aerosols from agricultural fires. They reported a high ratio of PM2.5 to PM10 (0.73) and concluded that soil dust was not a dominant aerosol in Phimai. They also analyzed the hygroscopic growth of observed aerosols. Tsuruta *et al* (2009) conducted continuous sampling observations at our Phimai site from July 2007 to June 2008 and analyzed chemical and element compositions of aerosols. They found that soil dust was a major aerosol component in both dry and wet seasons. Analyses by Tsuruta *et al* also indicated no significant difference in aerosol composition between the dry and wet seasons.

In this paper, we report the results of continuous observations using the lidar and the sky radiometer. We derived extinction coefficients of non-spherical aerosols (e.g., soil dust) and spherical aerosols (e.g., organic carbon (OC) and sulfate) separately, using the lidar depolarization ratio. We analyzed the dust events observed in the non-spherical aerosol time–height indications and confirmed the potential importance of long-range transported dust. We then focused our analysis on 2012 and 2013 where Raman scattering data were available. The contrast between 2012 and 2013 was also interesting because precipitation in the wet season of 2013 was higher than that of 2012, and precipitation in the dry season of 2013 was lower than that of 2012. We determined the difference in distribution patterns of non-spherical and spherical aerosols using composite diurnal variations of extinction coefficients. We also presented seasonal variations of the lidar ratio and extinction coefficient observed with the Raman lidar and the optical parameters derived from the sky radiometer data.

2. Observation

2.1. Lidar

The lidar used in the observation was a two-wavelength (532 and 1064 nm) lidar with a polarization-sensitive detector at 532 nm and a Raman scattering detector at 607 nm for receiving nitrogen vibrational Raman scattering excited at 532 nm. Transmitted laser energy was 20 (20) mJ/pulse at 532 (1064) nm, and the pulse repetition was 10 Hz. Analog detection was used for Mie-scattering channels and photon counting was used for the Raman scattering channel (Sugimoto *et al* 2008, Xie *et al* 2008). The lidar was operated so that it worked 5 min and paused 10 min. Signals were accumulated for 3000 laser shots, corresponding to 5 min. The profiles were recorded up to 24 km (30 km) with a vertical resolution of 6 m (30 m) for Mie-scattering (Raman-scattering) signals. The Raman detection channel was used only in the nighttime because the Raman signal was affected by daytime solar background radiation. Lidar observation was performed continuously, regardless of weather, through a glass window on the roof of the observation room. The lidar was maintained twice a year on average, and the calibration data were taken during the maintenance. The rate of operation of the lidar was 0.70 in 2005, 0.03 in 2006, 0.51 in 2007, 0.82 in 2008, 0.78 in 2009, 0.74 in 2010, 0.92 in 2011, 0.94 in 2012 and 0.96 in 2013.

We applied the standard data analysis method of AD-Net (Shimizu *et al* 2010) to the Mie-scattering and depolarization ratio data to derive extinction coefficient estimates for non-spherical and spherical aerosols. In this method, two types of aerosols having different depolarization ratios (different non-sphericity) are considered, and the observed aerosol is described as an external mixture of the two types (Sugimoto *et al* 2003, Shimizu *et al* 2004). The major component of non-spherical aerosols is soil dust. Spherical aerosols include sulfate, OCs, and sea salt. This method is useful for visualizing distributions of the two types of aerosols. Note, however, that some spherical aerosols (e.g., smoke) exhibit small non-sphericity (Sugimoto *et al* 2010, Tesche *et al* 2011), and they may appear as both non-spherical and spherical.

In the data analysis, clouds, fog, and heavy rain were detected before applying an inversion method to derive aerosol profiles. Cloud base height was defined as the height where the upward gradient of the attenuated backscattering coefficient (ABC) at 1064 nm exceeds an empirical threshold (2×10^{-8} m^{-2} sr^{-1}). The apparent cloud top was defined as the upper boundary where the ABC was equal to that of the corresponding cloud base. If the maximum of the ABC between the determined cloud base and the cloud top was less than a threshold (5×10^{-6} m^{-1} sr^{-1}), the layer was not marked as cloud. Water clouds and ice clouds were distinguished by the depolarization ratio. If the volume depolarization ratio at the detected cloud layer exceeded 0.2, the cloud was classified as an ice cloud. The backward Fernald method with a constant lidar ratio (extinction to backscatter ratio) was used to derive aerosol extinction coefficient profiles. We used the lidar ratio of 50 sr. The two-component method was then applied to separate non-spherical and spherical aerosols. The temporal resolution of the analysis

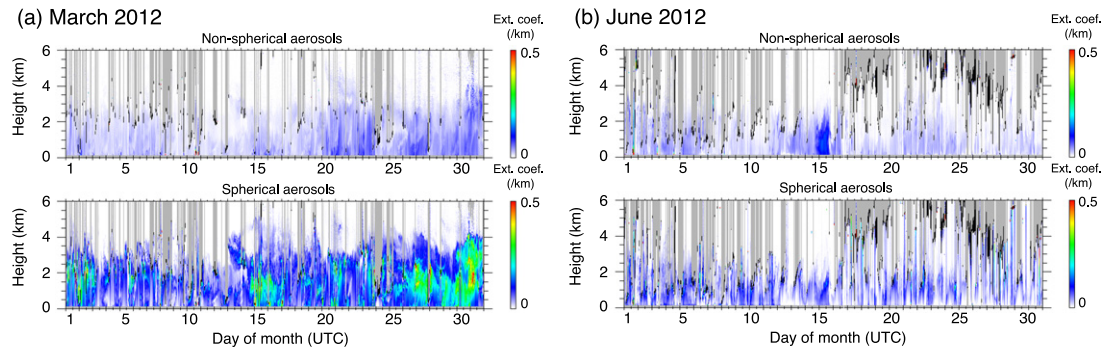

Figure 1. Time height indications of the extinction coefficient at 532 nm for non-spherical (upper) and spherical (lower) aerosols in March 2012 (left) and June 2012 (right).

was 15 min, and the height resolution was 30 m. The error in the two-component method depends on the density of aerosols, as discussed in our previous paper (Shimizu *et al* 2011). For low density, the error is due mainly to the error in the lidar ratio.

Aerosol extinction coefficient, backscattering coefficient, and consequently lidar ratio were derived from the Raman scattering signals. The extinction coefficient at 532 nm was derived from attenuation of the vibrational Raman scattering signal from atmospheric nitrogen molecules at 607 nm. We corrected the wavelength dependence of the aerosol extinction coefficient assuming that the Angstrom exponent is 1.0. We used the standard atmosphere (McClatchey *et al* 1972) for vertical profiles of nitrogen molecules. The backscattering coefficient was derived from the ratio of the Mie-scattering signal to the Raman-scattering signal (Xie *et al* 2008). The temporal resolution of the analysis was 15 min, and the height resolution was 120 m.

2.2. Sky radiometer

Observations were performed with a POM-02 sky radiometer (Prede Co. Ltd, Japan), and the aerosol optical parameters such as AOD, Angstrom exponent, and single-scattering albedo (SSA) were derived with SKYRAD.pack version 4.2 (Nakajima *et al* 1996, Takamura and Nakajima 2004). We used level 2 data including calibration using the improved Langley method and cloud screening (http://atmos.cr.chiba-u.ac.jp). The sky radiometer has been in operation in Phimai since 2005. However, the amount of available data was not sufficient for event analysis or even for discussing year-to-year variation. In this paper, we use the sky radiometer data only to discuss general seasonal variation of the aerosol optical parameters.

3. Results and discussion

3.1. Vertical distributions of non-spherical and spherical aerosols

Figure 1 presents examples of extinction coefficient estimates for non-spherical and spherical aerosols

Table 1. Long-range transported dust events observed in Phimai since 2007.

Year	Month	Day	Probable source area	Peak ext. coeffi. (km^{-1})
2008	March	2–6	Gobi	0.10
2009	March	15–17	Gobi	0.12
2009	April	24–25	Sahara?	0.10
2010	March	26–27	Gobi	0.07
2010	November	4	Gobi	0.16
2012	June	15	Sahara and/or Arabian peninsula	0.11
2013	April	6–9	Gobi	0.08
2014	June	21	Sahara	0.09

using the AD-Net data processing algorithm. Smoke plumes are observed in March in the spherical aerosol plot, and a dust event on 15 June 2012 is apparent in the non-spherical aerosol plot. Smoke plumes were often observed in the dry season, while dust events were occasionally observed. The dust event of 15 June was reproduced qualitatively in the time–height section archive product of the NAAPS model of the US Naval Research Laboratory (http://nrlmry.navy.mil/aerosol/#currentaerosolmodeling). A back-trajectory analysis using the NOAA HYSPLIT model (http://ready.arl.noaa.gov/HYSPLIT.php) suggested that the dust was transported across the Indian Ocean. Emissions of dust were confirmed in the NAAPS archives at the corresponding timing in the Saharan region of Africa and the Arabian Peninsula. The dust plume was also observed with CALIPSO/CALIOP over the Indian Ocean in several satellite paths (http://calipso.larc.nasa.gov/products/lidar/browse_images/production/).

Table 1 lists long-range transported dust events observed with the lidar in Phimai since 2007. All events listed were reproduced in the NAAPS time–height sections. Asian dust generated in the Gobi Desert in Northwest China and/or South Mongolia was sometimes transported to the

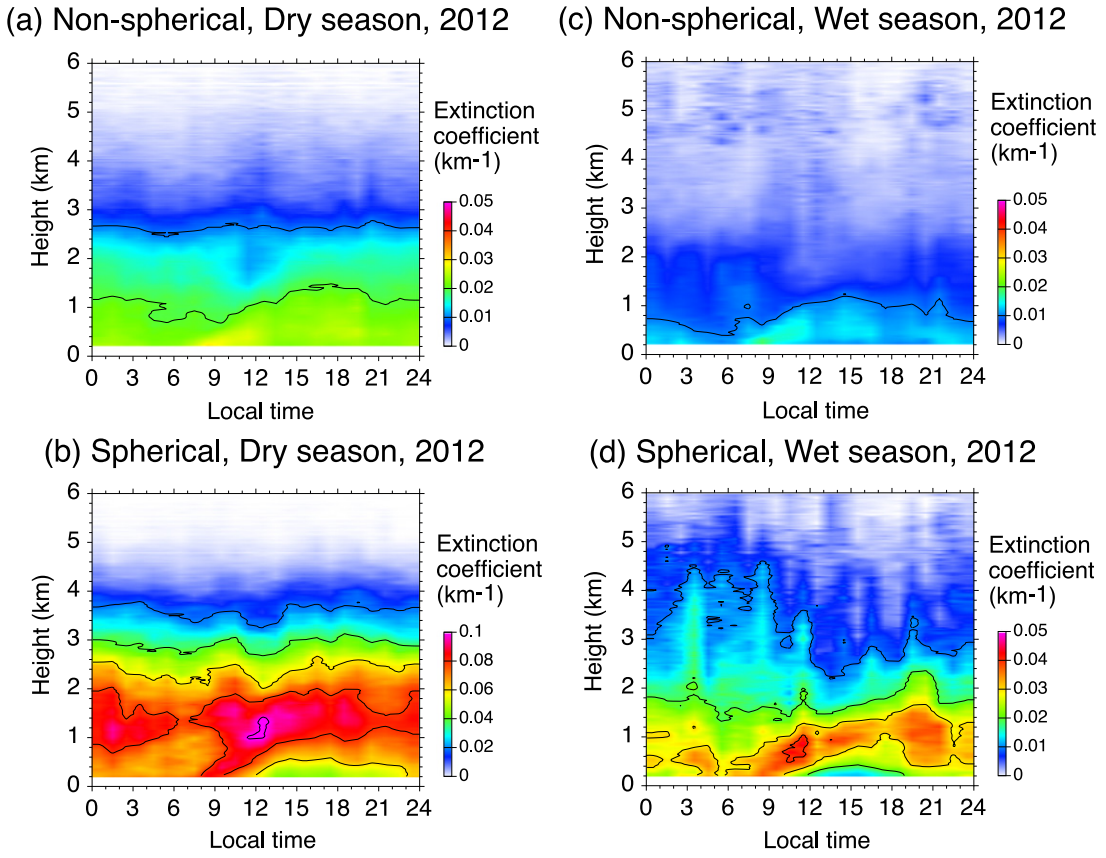

Figure 2. Composite diurnal variations of the extinction coefficient of non-spherical (dust) particles (upper) and spherical particles (lower) at 532 nm for (a) dry season (March–May) and (b) wet season (July–September) in 2012.

Southeast and occasionally reached Thailand from the Northeast. Dust from the Saharan area in Africa and from the Arabian Peninsula was also occasionally transported to Thailand from the West. Table 1 also lists probable source areas inferred from NAAPS and HYSPLIT trajectories, as well as peak extinction coefficients.

Dust events were not frequent; however, low-concentration non-spherical particles were almost always observed in the atmospheric mixing layer, as can be seen in the non-spherical aerosol plots in figure 1. Though smoke particles can exhibit small non-sphericity, the contribution of smoke in the non-spherical aerosol extinction coefficient is considered negligible, because the distribution patterns of non-spherical and spherical aerosols were different. Distribution of non-spherical aerosols had clear diurnal variation exhibiting the structure of the atmospheric mixing layer, while plumes of spherical particles were lifted in the mixing layer and residual layer. Some of the weak dust events (e.g. from 20 March to 31 in figure 1(a)) were qualitatively reproduced in the NAAPS time–height sections, and the contributions of transported dust were suggested.

Figures 2 and 3 illustrate composite diurnal variations of the extinction coefficient of non-spherical and spherical aerosols in the dry and wet seasons in 2012 and 2013. In both dry and wet seasons, non-spherical particles (dust) were distributed in the mixing layer and exhibited clear diurnal variation. Spherical aerosols also exhibited diurnal variation, but distributed differently. The difference in distribution is probably due to hygroscopic growth of spherical aerosol particles near the top of the mixing layer, where relative humidity is high. Another factor is the buoyancy of smoke plumes.

The distribution patterns in 2012 and 2013 are similar, although the density of near-surface spherical aerosol in the morning is much higher in the dry season of 2013. In 2012, the averaged extinction coefficient (km^{-1}) in the dry (wet) season at a height of 240 m was 0.024 (0.012) for non-spherical particles and 0.061 (0.025) for spherical particles. In 2013, it was 0.024 (0.012) for non-spherical particles and 0.123 (0.029) for spherical particles. The average extinction coefficient of spherical aerosols in the dry season was twice as high in 2013 than in 2012. It is probably linked to low precipitation in the dry season of 2013.

Figure 4 plots monthly precipitation in Nakhon Ratchasima (102.08 E, 14.97 N, 180 m ASL) near Phimai from 2008 to June 2014. In July 2011, precipitation was high, and a flood struck Bangkok. Total precipitation in the Phimai area, however, was higher

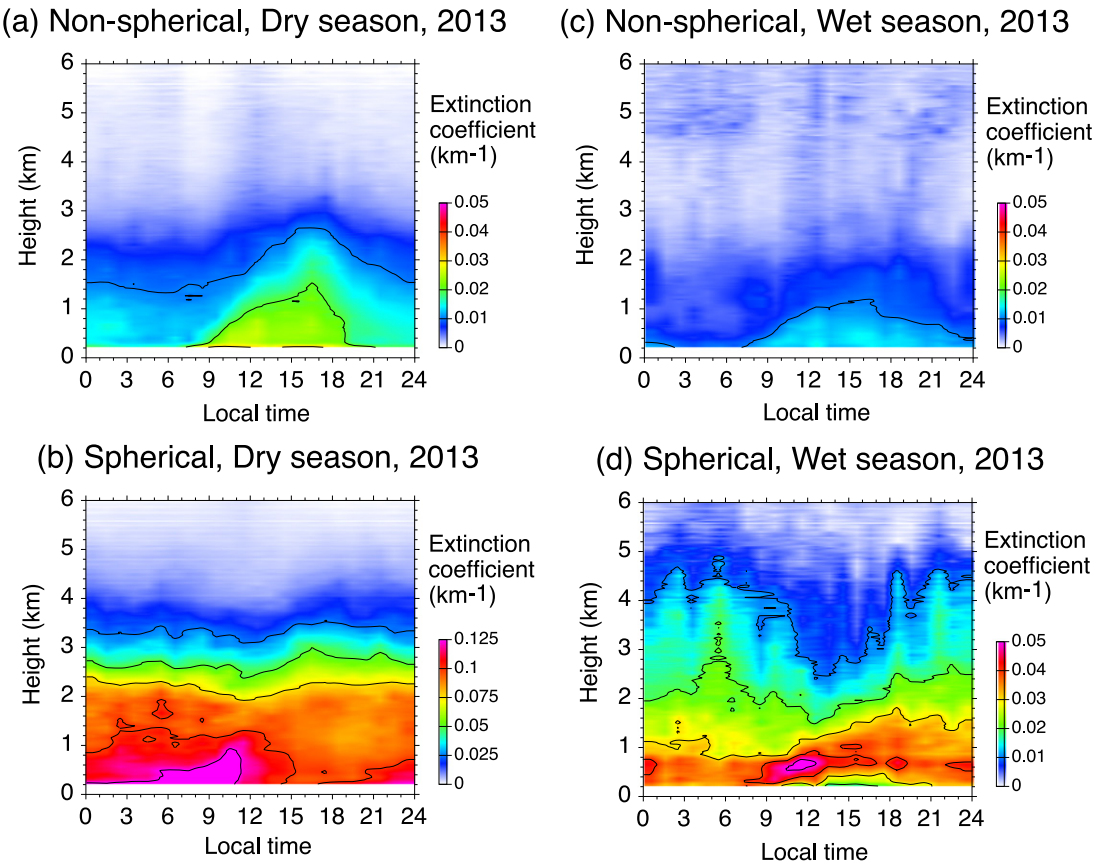

Figure 3. Same as figure 2 but for 2013.

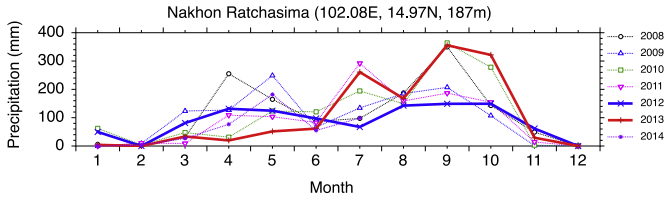

Figure 4. Monthly precipitation in Nakhon Ratchasima taken from the SYNOP reports.

in 2013. In contrast, precipitation in the dry season of 2013 was the lowest. In 2012, precipitation in the dry season was average, and it was lowest in the wet season.

The number of fires in the area of 9-22 N and 97-110 E extracted from the MODIS Active Fire Detections MCD14ML data distributed by NASA FIRMS (https://earthdata.nasa.gov/active-fire-data#tab-content-6) was 82 131 (95 189) in the dry season (March–May) in 2012 (2013) and 1470 (1157) in the wet season (July–September). The higher number of fires in the dry season of 2013 is consistent with the larger extinction coefficient. The number of fires in the wet season was 1.2–1.8% of that in the dry season; however, the extinction coefficient of spherical aerosols in the wet season was 24–40% of that in the dry season. This result suggests the contributions of other emission sources (e.g. households and vehicles) in the wet season.

The existence of soil dust in both the dry and wet seasons is consistent with chemical and element analyses performed in 2007 through 2008 by Tsuruta *et al* (2009). They reported that 38% (48%) of PM10 was soil dust in the dry (wet) season. The ratios of elemental carbon (EC), OC, sulfate, dust, nitrate and sea salt in PM10 in the dry (wet) seasons estimated from the data of Tsuruta *et al* (2009) were 0.07 (0.05), 0.25 (0.22), 0.26 (0.17), 0.38 (0.48), 0.02 (0.05), and 0.02 (0.03). The ratios of EC, OC, and sulfate were slightly higher in the dry season, and those of dust, nitrate and sea salt were higher in the wet season. A low concentration of biomass burning-originated potassium was observed in the dry season. PM10 ($\mu g\,m^{-3}$) was 32.7 (14.4) in the dry (wet) season, and the dust

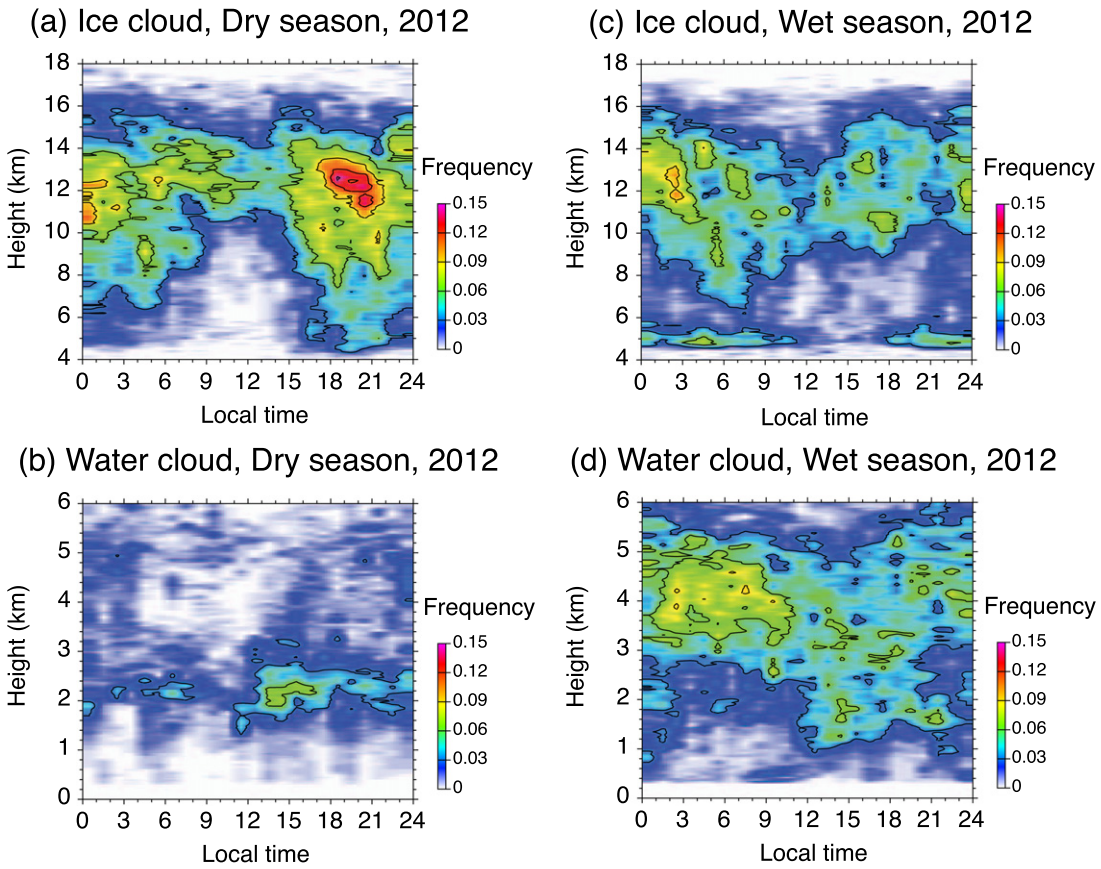

Figure 5. Composite diurnal variations of the frequency of ice cloud (upper) and water cloud (lower) in (a) dry season (March–May) and (b) wet season (July–September) in 2012.

concentration in PM10 (μg m^{-3}) was 12.4 (6.8) in the dry (wet) season. The PM2.5 to PM10 ratio estimated from their report was 0.72 in the dry season and 0.56 in the wet season. This value in the dry season was close to the ratio of 0.73 that reported by Li *et al* (2013). The ratio of the dust concentration in PM2.5 to the dust concentration in PM10 estimated from the Tsuruta's report is 0.49 (0.43) in the dry (wet) season. This value is too large for locally generated dust; however, it is possible for long-range transported dust or reemitted transported dust.

Although the existence of dust in the mixing layer is evident from Tsuruta's report and the lidar data in figures 2 and 3, the detailed mechanism of the transport of dust particles (e.g. advection, convection, deposition, and re-emission) is still not clear. Surface wind speed was generally low; however dust deposited on the ground may be reemitted without saltation (Loosmore and Hunt 2000). If deposition and reemission are involved, the interaction of dust and biological and organic materials is an interesting subject of study. This interaction may enhance the ice nucleation ability of dust particles (Hoose *et al* 2010, Tobo *et al* 2014, DeMott *et al* 2015, Mamouri and Ansmann 2015). To clarify the transport mechanism of dust in the mixing layer, high temporal resolution measurements of concentration and size distribution of dust particles are required. We are planning observations in Phimai using a polarization particle counter that can measure size and non-sphericity of single particles with a high temporal resolution (Kobayashi *et al* 2014, Sugimoto *et al* 2015).

3.2. Cloud vertical distributions

It would be interesting to study cloud distributions observed with the lidar. Figures 5 and 6 depict diurnal variation of frequencies of ice and water clouds. The frequency is defined so that it is 1 when cloud is always observed at that altitude. We must note, however, that the lidar signals are attenuated with scattering by clouds; consequently, only portions of clouds near the cloud base are correctly detected. The frequency above dense cloud was underestimated.

Comparing 2012 and 2013, a difference is observed in high-altitude ice cloud in the dry season and low-altitude water cloud in the wet season. In the wet season of 2013, the frequency of low-water cloud was significantly high, probably due to high-concentration spherical aerosols (figure 3(d)) that may act as condensation nuclei. However, the dense low clouds did not cause precipitation. Most of the precipitation was from deep convective ice clouds,

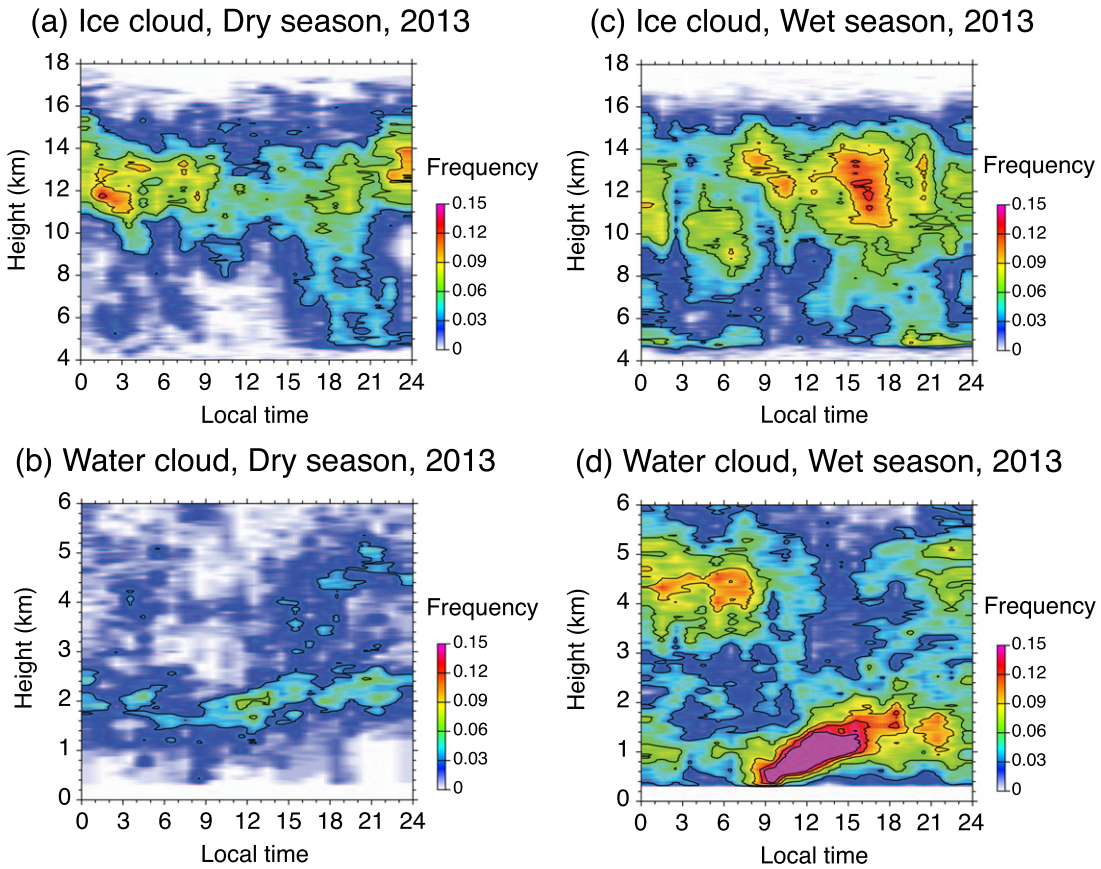

Figure 6. Same as figure 5 but for 2013.

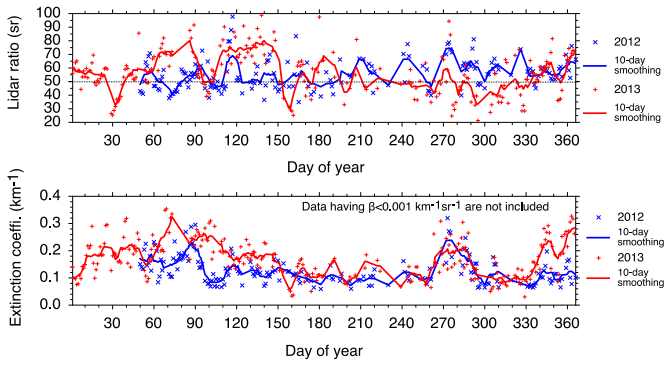

Figure 7. Variation of daily lidar ratio (upper) and daily extinction coefficient (lower) averaged at 60–2400 m height derived from the Raman lidar data.

although only cloud base portions are represented in figures 5 and 6. The melting layer is observed at 4.6 km height.

Using the current cloud detection algorithm, rain below ice clouds is sometimes misclassified as water cloud. Another problem with the current cloud and rain detection algorithm is that rain is sometimes classified as spherical aerosols. The distribution of spherical aerosols above 2.5 km in the wet season in figures 2 and 3 is probably contaminated by misclassified rain.

3.3. Optical characteristics of aerosols and their seasonal variations

Aerosol events like those represented in figure 1 were also observed with the Raman receiver, and the extinction coefficient and the lidar ratio were derived. To study seasonal variation, we plot temporal variation of daily lidar ratio and extinction coefficient in the boundary layer in figure 7. The daily lidar ratio is defined as the ratio of averaged extinction coefficient to averaged backscattering coefficient in the nighttime at heights of 60–2400 m. Both lidar ratio and

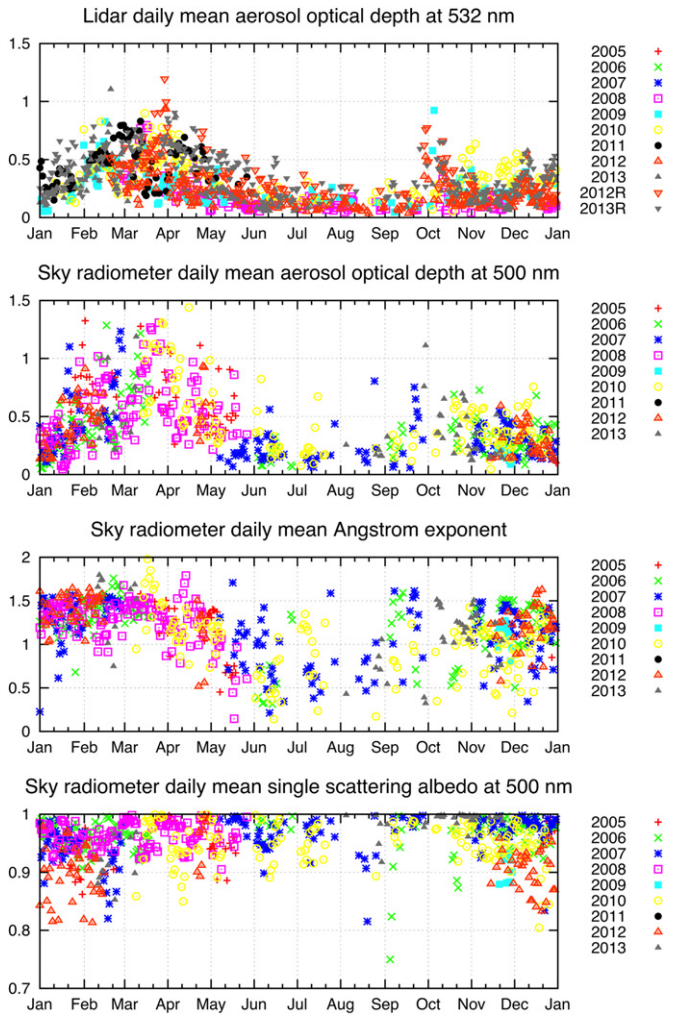

Figure 8. Seasonal variations of aerosol optical properties observed with the lidar and the sky radiometer in Phimai.

extinction coefficient were higher in the dry season and lower in the wet season, especially in 2013. The lidar ratio and extinction coefficient in the dry season of 2013 were higher than those of 2012, which can be linked to a higher number of biomass-burning events due to the low precipitation in 2013.

Figure 8 indicates seasonal variations of AOD obtained from the Mie-lidar extinction coefficient profile from 120 m to 6 km, sky radiometer daily AOD, Angstrom exponent, and SSA. The AOD derived from the Raman-lidar extinction coefficient profile from 120 m to 6 km is also indicated for 2012 and 2013 in the top panel. The Mie-lidar AOD is smaller than the Raman-lidar AOD, reflecting the error in the constant lidar ratio (50 sr) assumption in the Mie-lidar data analysis. Although there was not enough sky radiometer data to discuss year-to-year variation, general features of seasonal variations are indicated in figure 8. AOD and Angstrom exponent were high in the dry season and low in the wet season. SSA was low in the dry season and high in the wet season. The seasonal variation of lidar ratio in figure 7 is consistent with that of SSA.

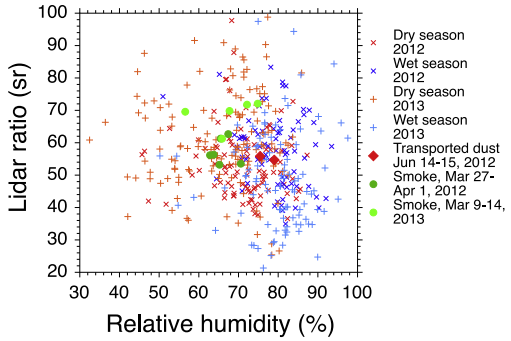

Figure 9. Scatter plot of the lidar ratio in figure 7 versus the ECMWF relative humidity data.

To analyze the aerosol characteristics in the dry and wet seasons, we made a scatter plot of the lidar ratio versus relative humidity (figure 9). We used ECMWF reanalysis humidity data at (102 E, 15 N) averaged at the corresponding height range (150–2350 m) in the nighttime. Data in the dry season (January–May and October–December) and the wet season (June–September) are indicated by different

colors in figure 9. The number of high (low) lidar ratio data was higher in the dry (wet) season. The low lidar ratio data may include large aerosols near cloud bases and misclassified rain.

In figure 9, the data points for three examples of aerosol events are indicated by different symbols and colors. For smoke from 27 March to 1 April in 2012, dependence of the lidar ratio on relative humidity may be seen, although we should be careful because we do not observe the same air mass at the different data points. Mie-scattering calculation based on the aerosol optical model used in the chemical transport model GEOSChem (http://acmg.seas.harvard.edu/geos/index.html) for OC and sulfate indicates that the lidar ratio generally increases when relative humidity increases. The calculated lidar ratio value depends on the mode radius of the assumed aerosol optical model. We may determine reasonable optical models by comparing the calculation with the observations for selected aerosol events. The calculation also indicates that the Angstrom exponent generally decreases when relative humidity increases. Relative humidity is an important factor also in the seasonal variation of the Angstrom exponent.

4. Conclusions

Continuous observations using the polarization lidar indicated that dust events were occasionally observed. Analysis using NAAPS and HYSPLIT suggested that dust was transported to Phimai from the Gobi Desert in Mongolia and/or China, the Sahara Desert in Africa, and the Arabian Peninsula. Analysis of the lidar data also indicated that a small amount of background dust was almost always found in the atmospheric mixing layer.

The results of the present study were consistent with the chemical and elemental analyses of aerosols in Phimai conducted in 2007 through 2008 by Tsuruta *et al* (2009). Their results indicated that the PM2.5 to PM10 ratio of soil dust was 0.4–0.5. This is considered too large for locally generated dust, and the origin of the fine dust particles is in question. Analysis of the lidar data using NAAPS indicated that there were very weak long-range transported dust events, and the long-range transported dust and reemission of the transported dust were considered sources of fine dust particles. The behavior of background dust in the atmospheric mixing layer (e.g. dust mass balance, advection, convection, deposition, reemission, and interaction with air pollution and organic materials) is still not well understood, and it would be an interesting subject for future studies.

Seasonal variations of the aerosol optical parameters derived from the Mie–Raman lidar and the sky radiometer were qualitatively explained by frequent biomass burning in the dry season. Contributions of other emission sources were also suggested from the lidar spherical-aerosol extinction coefficient in the wet seasons where the number of biomass-burning fires was very small.

References

Campbell J R *et al* 2012 Characterizing the vertical profile of aerosol particle extinction and linear depolarization over Southeast Asia and the maritime continent: the 2007–2009 view from CALIOP *Atmos. Res.* **122** 520–42

DeMott P J *et al* 2015 Integrating laboratory and field data to quantify the immersion freezing ice nucleation activity of mineral dust particles *Atmos. Chem. Phys.* **15** 393–409

Hoose C, Kristjansson J E and Burrows S M 2010 How important is biological ice nucleation in clouds on a global scale? *Environ. Res. Lett.* **5** 024009

Kobayashi H *et al* 2014 Development of a polarization optical particle counter capable of aerosol type classification *Atmos. Environ.* **97** 486–92

Li C *et al* 2013 Characteristics and composition of atmospheric aerosols in Phimai, central Thailand during BASE-ASIA *Atmos. Environ.* **78** 60–71

Lin N-H *et al* 2013 An overview of regional experiments on biomass burning aerosols and related pollutants in Southeast Asia: from BASE-ASIA and the dongsha experiment to 7-SEAS *Atmos. Environ.* **78** 1–19

Loosmore G A and Hunt J R 2000 Dust resuspension without saltation *J. Geophys. Res.* **105** 20663–71

Mamouri R E and Ansmann A 2015 Estimated desert–dust ice nuclei profiles from polarization lidar: methodology and case studies *Atmos. Chem. Phys.* **15** 3463–77

McClatchey R A, Fenn R W, Selby J E A, Volz F E and Garling J S 1972 *Optical Properties of the Atmosphere* 3rd edn AFCRL Environ. Res. Pap. vol 411 (Bedford, MA: Air Force Cambridge Res. Lab.) p 108

Nakajima T, Tonna G, Rao R, Kaufman Y and Holben B 1996 Use of sky brightness measurements from ground for remote sensing of particulate polydispersions *Appl. Opt.* **35** 2672–86

Nakajima T *et al* 2007 Overview of the atmospheric brown cloud East Asian regional experiment 2005 and a study of the aerosol direct radiative forcing in East Asia *J. Geophys. Res.* **112** D24S91

Shimizu A, Sugimoto N and Matsui I 2006 Seasonal and inter-annual variations of vertical aerosol distribution observed in Thailand *Proc. 23rd Int. Laser Radar Conf.* pp 801–4

Shimizu A, Sugimoto N and Matsui I 2010 Detailed description of data processing system for lidar network in East Asia *Proc. 25th Int. Laser Radar Conf.* pp 911–3

Shimizu A, Sugimoto N, Matsui I, Arao K, Uno I, Murayama T, Kagawa N, Aoki K, Uchiyama A and Yamazaki A 2004 Continuous observations of Asian dust and other aerosols by polarization lidar in China and Japan during ACE-Asia *J. Geophys. Res.* **109** D19S17

Shimizu A, Sugimoto N, Matsui I, Mori I, Nishikawa M and Kido M 2011 Relationship between lidar-derived dust extinction coefficients and mass concentrations in Japan *SOLA* **7A** 001–004

Sugimoto N, Matsui I, Shimizu A, Nishizawa T, Hara Y, Xie C, Uno I, Yumimoto K, Wang Z and Yoon S-C 2008 Lidar network observations of tropospheric aerosols *Proc. SPIE* **7153** 71530A

Sugimoto N, Nishizawa T, Shimizu A, Matsui I and Jin Y 2014 Characterization of aerosols in East Asia with the Asian dust and aerosol lidar observation network (AD-Net) *Proc. SPIE* **9262** 92620K

Sugimoto N, Nishizawa T, Shimizu A, Matsui I and Kobayashi H 2015 Detection of internally mixed Asian dust with air pollution aerosols using a polarization optical particle counter and a polarization-sensitive two-wavelength lidar *J. Quant. Spectrosc. Radiat. Transfer* **150** 107–13

Sugimoto N, Tatarov B, Shimizu A, Matsui I and Nishizawa T 2010 Optical characteristics of forest-fire smoke observed with

two-wavelength Mie-scattering lidars and a high-spectral-resolution lidar over Japan *SOLA* **6** 093–6

Sugimoto N, Uno I, Nishikawa M, Shimizu A, Matsui I, Dong X, Chen Y and Quan H 2003 Record heavy Asian dust in Beijing in 2002: observations and model analysis of recent events *Geophys. Res. Lett.* **30** 1640

Takamura T and Nakajima T 2004 Overview of SKYNET and its activities *Opt. Pura Apl.* **37** 3303–8

Tesche M, Gross S, Ansmann A, Muller D, Althausen D, Freudenthaler V and Esselborn M 2011 Profiling of Saharan dust and biomass-burning smoke with multiwavelength polarization Raman lidar at Cape Verde *Tellus* **63B** 649–76

Tobo Y, DeMott P J, Hill T C J, Prenni J A, Swoboda-Colberg N G, Franc G D and Kreidenweis S M 2014 Organic matter matters for ice nuclei of agricultural soil origin *Atmos. Chem. Phys.* **14** 8521–31

Tsuruta H *et al* 2009 Chemical characterization of atmospheric aerosols at Phimai, Thailand: II. Contribution of fossil fuel combustion, biomass burning, and soil dust *NMCC Ann. Rep.* **16** 152–62 (in Japanese)

Xie C, Nishizawa T, Sugimoto N, Matsui I and Wang Z 2008 Characteristics of aerosol optical properties in pollution and Asian dust episodes over Beijing, China *Appl. Opt.* **47** 4945–51